Eur Biophys J (2009) 38:1061–1068
DOI 10.1007/s00249-009-0509-y

ORIGINAL PAPER

Ca^{2+} spiral waves in a spatially discrete and random medium

Jun Tang · Lijian Yang · Jun Ma · Ya Jia

Received: 6 April 2009 / Revised: 8 June 2009 / Accepted: 10 June 2009 / Published online: 7 July 2009
© European Biophysical Societies' Association 2009

Abstract It is well known that the spatial distribution of the calcium ion channels in the endoplasmic reticulum is discrete. We study the Ca^{2+} spiral pattern formation based on a model in which ion channels are discretely and randomly distributed. Numerical simulations are performed on different types of media with the Ca^{2+} release sites uniformly distributed, discretely and uniformly arranged, or discretely and randomly arranged. The comparisons among the different media show that random distribution is necessary for spontaneous initiation of Ca^{2+} spiral waves, and the discrete and random distribution is of significance for spiral waves under physiologically reasonable conditions. The period and velocity of spiral waves are also calculated, and they are not prominently changed by varying the type of medium.

Keywords Ca^{2+} spiral waves · Ion channel · Random medium

Introduction

Ca^{2+} is used as a second messenger in cell signalling. Most of the calcium ions that constitute the signal are released from intracellular stores, e.g., the endoplasmic reticulum (ER) or sarcoplasmic reticulum (SR), in which the normal Ca^{2+} concentration is much higher than that of cytosol inside the intracellular space. Ca^{2+} is released from intracellular stores through two types of ion channels: the ryanodine receptor (RyR) and the inositol 1,4,5-trisphosphate receptor (IP_3R). Ca^{2+} cannot transmit information by its binding specificity or simply by its presence. Consequently, the signal is encoded in temporal and spatial patterns, such as Ca^{2+} waves (Falcke 2004). Intracellular calcium waves were first observed in medaka eggs (Ridgway et al. 1977) and then found in *Xenopus* oocytes and other cell types (Sanderson et al. 1994; Robb-Gaspers and Thomas 1995; Thomas et al. 1995; Harris-White et al. 1998; Lipp and Niggli 1993).

In *Xenopus* oocytes, IP_3R is the only type of ion channel in the ER. It is widely accepted that the release channels are spatially organized in clusters, and there are only a few tens of intact IP_3 receptor channels in square-micrometer-sized clusters (Bootman et al. 1997; Foskettet et al. 2007). Many effects of this type of discrete distribution of ion channels in the ER have been experimentally studied. The most prominent one is the transition from local calcium release to calcium wave propagation (Parker and Yao 1991; Yao et al. 1995; Parker and Yao 1996; Yagodin et al. 1995, 1994; Cheng et al. 1996). For example, in *Xenopus* oocytes, with low IP_3 concentration, Ca^{2+} puffs—Ca^{2+} releasing from the serval ion channel in a cluster—are observed. As IP_3 concentration increases above a threshold value, a Ca^{2+} wave is able to propagate from the site of the initial Ca^{2+} release (Parker and Yao 1991, 1996; Yao et al. 1995). Furthermore, it is known that the discrete release sites are randomly arranged in the ER. To our knowledge, the effects of the random distribution of Ca^{2+} release sites have not been extensively studied. Bugrim

J. Tang (✉)
College of Science, China University of Mining and Technology, 221008 Xuzhou, China
e-mail: tjuns1979@yahoo.com.cn

J. Tang · L. Yang · J. Ma · Y. Jia
Department of Physics and Institute of Biophysics, Huazhong Normal University, 430079 Wuhan, China

J. Ma
Department of Physics, Lanzhou University of Technology, 730050 Lanzhou, China

et al. (1997) presented a model with a random spatially discrete distribution of Ca^{2+} release sites, but they did not focus on the effect of the randomness.

In 1991, Lechleiter et al. (1991a, b) discovered Ca^{2+} spiral waves in immature oocytes, and later on, spiral waves were also observed in other cell types, such as cardiac cells. The propagation of spiral waves has been extensively simulated by considering the diffusion of cytosolic Ca^{2+} in various models initially developed to account for Ca^{2+} oscillations in homogeneous conditions (Falcke et al. 1999a, b; Dupont 1998). Based on these models, the initiation of spiral waves has been studied, and many experimental results about the period and velocity of spiral waves have been reproduced (Falcke et al. 1999a, b, 2003; Tang et al. 2008). To study the effect of discrete distribution of Ca^{2+} release sites on Ca^{2+} spiral waves, Falcke et al. present a heterogeneous model in which release sites are regularly arranged on a hexagonal grid (Falcke 2003). But as mentioned above, the release sites are randomly distributed in the ER, so a question to be raised is as follows: does the random distribution of release sites play some significant role in the initiation and propagation of the Ca^{2+} spiral wave? To account for the effects of random and discrete distribution of Ca^{2+} release sites on the Ca^{2+} spiral waves, in this paper, based on a model presented by Bugrim et al. (1997), the Ca^{2+} spiral waves are compared in different types of media with the Ca^{2+} release sites uniformly distributed, discretely and uniformly arranged, or discretely and randomly arranged. Our results show the randomness and discreteness of the distribution of release sites is important for initiation and propagation of Ca^{2+} spiral waves, therefore it is necessary to consider them when modelling Ca^{2+} spiral waves.

Model and simulation

There are a number of models for studying the local dynamics of cytosolic Ca^{2+} concentration, all of which show a great deal of fundamental similarity (De Young and Keizer 1992; Li and Rinzel 1994; Tang et al. 1996). Here we shall use a simplified model that takes into account only the exchange between the cytoplasm and the ER. It contains three fluxes across the ER membrane: release through the ion channels (IP_3Rs), removal of Ca^{2+} by an ATP-dependent pump, and a leak (Bugrim et al. 1997).

The flux through the ion channels is determined by the state of receptor, which in turn is determined by the binding of IP_3 or Ca^{2+} to the receptor. Each receptor has four identical subunits and every subunit has three binding sites: a site for IP_3, an activating site, and an inactivating one for Ca^{2+} (Foskett et al. 2007). In order for a subunit to be activated, only the IP_3 and the activating Ca^{2+} binding site need to be occupied, then for the ion channel to be open, at least three of the four subunits are activated. In keeping with the De Young-Keizer model, we allow the parallel binding and dissociation at all sites of the subunits. Under the assumption that the rate constants do not depend on the state of the receptor, the equations defining the local dynamics of the active sites where the discrete ion channels and pumps are distributed are as follows (Bugrim et al. 1997):

$$\begin{aligned}\frac{dC}{dt} &= \left[P_l + \frac{P_c I C(1-v)}{(1+k_0 I/k_{-0})(1+k_1 C/k_{-1})}\right](C_R - C) \\ &\quad - P_p \frac{C^2}{C^2 + K_C^2}, \\ \frac{dv}{dt} &= k_2 C(1-v) - k_{-2} v,\end{aligned} \tag{1}$$

where C and C_R denote the Ca^{2+} concentration in the cytosol and ER, respectively, and v is the fraction of inhibited ion channels. The values and definitions of the parameters are listed in Table 1 (Bugrim et al. 1997).

In Eqs. 1, the density of active sites is equal to 1. Obviously, for the sites without ion channels and pumps, termed passive sites, the density should be equal to 0. To simulate a cell with both active sites and passive sites, a function $f(x,y)$ is introduced. Within the areas occupied by the active sites, $f(x,y) = 1$, and for the passive sites $f(x,y) = 0$. A diffusive term is added to Eqs. 1, and the spatially extended model is given by Bugrim et al. (1997):

$$\begin{aligned}\frac{dC}{dt} &= \left[P_l + \frac{P_c [IP_3] C(f(x,y) - v)}{(1+k_0[IP_3]/k_{-0})(1+k_1 C/k_{-1})}\right](C_R - C) \\ &\quad - f(x,y) P_p \frac{C^2}{C^2 + K_C^2} + D_{\text{eff}} \nabla^2 C, \\ \frac{dv}{dt} &= k_2 C(1-v) - k_{-2} v\end{aligned} \tag{2}$$

For simplification, Eqs. 2 are normalized to dimensionless equations:

$$\begin{aligned}\frac{du}{d\tau} &= \frac{1}{\varepsilon}\left[\alpha_1(1-u) + \alpha_2(1-u)\frac{u(f(x,y)-v)}{(1+\beta_0)(u+\beta_1)}\right. \\ &\quad \left. - \frac{u^2}{u^2 + \alpha_3^2} f(x,y)\right] + \nabla^2 u, \\ \frac{dv}{d\tau} &= -v + \frac{u}{\beta_2}(f(x,y) - v),\end{aligned} \tag{3}$$

where $u = C/C_m$ represents the dimensionless concentration of cytosol Ca^{2+}, the fraction of inhibited ion channel is denoted by v, and τ is the effective time. The parameters in the dimensionless model are calculated as shown in Table 2 (Bugrim et al. 1997). To understand the normalization in more detail, see Bugrim et al. (1997).

Table 1 Parameters of the model

Constant	Definition	Value
γ	ER volume/cytoplasmic volume	0.185
P_c	Channel conductance rate constant	3.7 s^{-1}
P_l	Leakage rate constant	0.00059 s^{-1}
P_p	Maximum pump rate	10.0 $\mu M\ s^{-1}$
K_C	Michaelis constant for the pump	0.03 μM
C_m	Average Ca^{2+} concentration	1.56 μM
k_0	IP_3 binding rate constant	96 $\mu M^{-1}\ s^{-1}$
k_1	Binding rate constant for activating Ca^{2+}	150 $\mu M^{-1}\ s^{-1}$
k_2	Binding rate constant for inhibiting Ca^{2+}	1.8 $\mu M^{-1}\ s^{-1}$
k_{-0}	IP_3 dissociation rate constant	9.6 s^{-1}
k_{-1}	Dissociation rate constant for activating Ca^{2+}	16.5 s^{-1}
k_{-2}	Dissociation rate constant for inhibiting Ca^{2+}	0.21 s^{-1}
D_{eff}	Effective diffusion coefficient of Ca^{2+} in cytoplasm	21 $\mu m^2\ s^{-1}$
$[IP_3]$	The concentration of IP_3	Varied

The simulations are performed on systems of 60 × 60 space units, which corresponds to the length scale of *Xenopus* oocytes. The boundary condition used here is the non-flux boundary condition. Equations 3 are integrated using a Euler forward scheme, with a spatial discretization of 0.1 space unit and a time step of 0.001 time unit. An important parameter p, the active site density, is introduced to represent the fraction of the active area where the ion channels are distributed. In *Xenopus* oocytes, p is about 0.13−0.16 (Bugrim et al. 1997).

To generate a system in which discrete active sites are randomly arranged, which will be called a random and discrete medium (RDM) in this paper, the system is divided into 300 × 300 squares. For every square, a uniform random number between 0 and 1 is produced and compared with p. If the random number is less than p, the corresponding square is assigned as an active site, i.e., $f(x,y) = 1$, otherwise, $f(x,y)$ is set to 0. To compare with RDM, a regular and discrete medium (RDcM) is generated by regularly arranging the active sites, and a homogeneous medium (HM) is generated by setting $f(x,y)$ to its mean value p everywhere in the medium.

Table 2 Dimensionless parameters

Constant	Definition
α_1	$(1+\gamma)P_l C_m/P_p\gamma$
α_2	$(1+\gamma)P_c C_m/P_p\gamma$
α_3	K_C/C_m
β_0	$k_{-0}/k_0[IP_3]$
β_1	$k_{-1}/k_1 C_m$
β_2	$k_{-2}/k_2 C_m$
ε	$k_{-2}C_m/P_p$

Results and discussion

Firstly, the numerical simulations are performed on RDM. We fix p and $[IP_3]$ at 0.15 and 0.4 μM, respectively; these values are both physiologically reasonable. The initial value of u is set to its stationary state, and then the system is disturbed with a local u increasing to 0.2 in the center of the system. This perturbation is strong enough to activate the medium which can be seen here as an excitable system. The perturbation with higher u increasing does not make a difference. For rather low $[IP_3]$ ($[IP_3] < 0.352$ μM), the perturbation is annihilated before propagating across the system (see the top row of Fig. 1). On the other hand, for very high $[IP_3]$ ($[IP_3] > 0.380$ μM), a plane wave initialized by the perturbation can successfully propagate across the system (see the bottom row of Fig. 1). These results are similar to Bugrim et al. (1997) and in keeping with experiments. In this paper, five random distributions for RDM were tested, and no significant difference was found.

It is intriguing that for $0.352\ \mu M < [IP_3] < 0.380\ \mu M$, the propagating plane wave is cut off into several segments, and the open ends of these segments curl up into spiral tips (see the center row of Fig. 1), which are topological defects in the system. These defects make the spiral waves permanently sustained in the system unless other perturbations are used. The system exhibits a well-known mechanism of spiral pattern initiation, and in some cell types, this mechanism has been proven to be used by Ca^{2+} spiral waves (Dupont 1998). For $[IP_3] < 0.352$ μM or $[IP_3] > 0.380$ μM, the system always recovers to rest states after several time units; in contrast, Ca^{2+} spiral waves are permanently sustained in the system for $0.352\ \mu M < [IP_3] < 0.380\ \mu M$. The Ca^{2+} concentrations at the selected point (50, 50) (indicated by a red arrow in Fig. 1) are plotted against time in Fig. 2. For low $[IP_3]$, no spiking happens because the Ca^{2+} wave fails to propagate to point (50, 50); for high $[IP_3]$, the selected point spikes only one time, which corresponds to the plane wave propagating to that point. Only for $0.352\ \mu M < [IP_3] < 0.380\ \mu M$ are persistent Ca^{2+} spikes found. It is more important that these persistent Ca^{2+} spikes are not unorderly, and a prominent peak value can be found in corresponding power spectral densities (PSD) (see Fig. 2d). This coherent spiking behavior allows the Ca^{2+} system to carry a signal.

Secondly, Ca^{2+} spiral waves will be modelled in RDM and HM from an unphysiological initial condition, termed

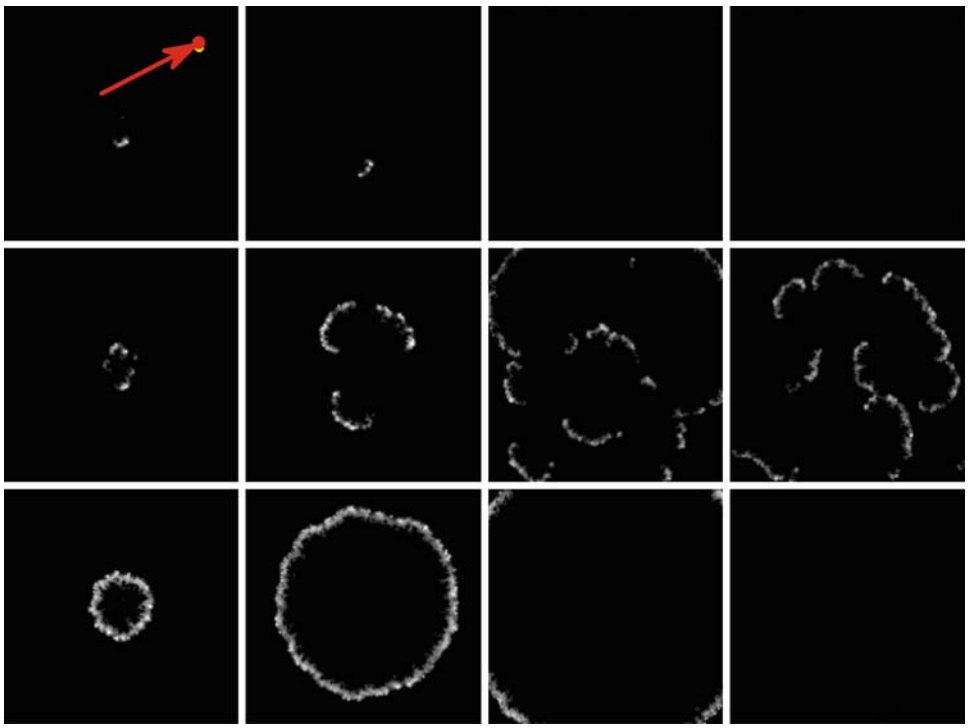

Fig. 1 Dynamics of Ca^{2+} waves for various [IP_3]. *Top row*: [IP_3] = 0.35 μM, *center row*: [IP_3] = 0.37 μM, and *bottom row*: [IP_3] = 0.50 μM. From *left to right*: for the first two rows, $t = 1$, 3, 7, and 10 time units; for the bottom row, $t = 1$, 3, 5, and 10 time units. The *black to white gray scale* represents the lowest value 0 to the highest value 0.32 of u. This *gray scale* will be used in all figures throughout this paper unless otherwise stated

the locally perturbed rest state. This initial condition is extensively used to develop spiral waves in excitable systems such as the BZ reaction system. The initial condition is that, in a square area, u decreases from left to right while v increases, and in positions out of the square area, all u and v are set at rest states (see Fig. 3).

By fixing the concentration of IP_3 at 0.4 μM and varying p, we performed simulations on RDM and HM. In HM, the spiral waves can develop from the initial condition and be permanently sustained in the medium for $0.626 < p < 1$. In *Xenopus* oocytes, p is about 0.13−0.16, i.e., the simulations in HM can not reproduce the Ca^{2+} spiral waves found in *Xenopus* oocytes. In RDM, the spiral waves can develop and be sustained for $0.116 < p < 1$, which includes physiologically reasonable values of p. Only for p close to 0.116 will the spiral waves break up and more tips form in RDM; for other values of p in this range, the sustained spiral wave has only one tip. The comparison between the two types of media tells us the discrete and random distribution of ion channels is significant for the reproduction of the Ca^{2+} spiral wave by this model scheme. Figure 4 gives an example of $p = 0.15$. In the top row of Fig. 4, the initial condition fails to develop a spiral wave in HM. In contrast, in the second row of Fig. 4, the Ca^{2+} spiral wave is successfully developed in RDM.

In Fig. 5, we also give an example of developing a spiral wave with an unphysiological p value in a homogeneous medium.

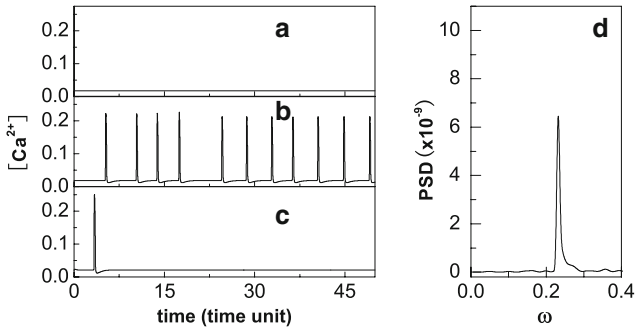

Fig. 2a–d Time evolutions of [Ca^{2+}] at point (50, 50) for various [IP_3]. **a** [IP_3] = 0.35 μM, **b** [IP_3] = 0.37 μM, **c** [IP_3] = 0.50 μM, **d** power spectral densities (PSD) of the time series in **b**

We have also compared the periods and velocities of Ca^{2+} spiral waves in RDM and HM. To calculate the period, one point in the medium is selected, and the power spectra of the time series is obtained; the period with highest amplitude is selected as the spiral of the spiral waves. The periods shown in Fig. 6a are averaged over 10 points, and averaging over more points does not result in a significant difference. The dependence of the average period on p is shown in Fig. 6a. The period ranges from seconds to tens of seconds (1 time unit = 5 s), which is in accordance with experiments and previous numerical works (Bugrim et al. 1997; Falcke et al. 1999a; Tang et al. 2008; Falcke 2003). For both types of media, the period of the Ca^{2+} spiral wave decreases with p, and the periods are almost the same in the two types of media at large values of

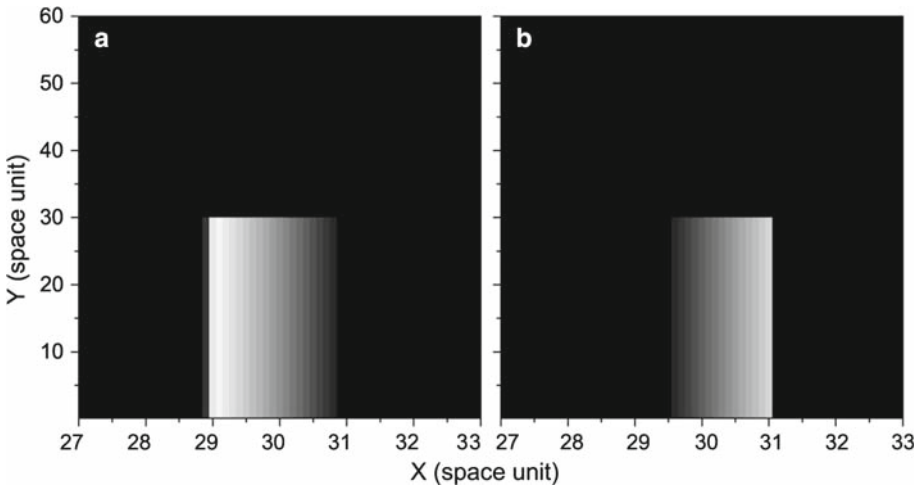

Fig. 3 The spatial formation of variable $u(x,y)$ (**a**) and $v(x,y)$ (**b**) in the unphysiological initial condition used to develop spiral waves. The gray scale in **a** is the same as Fig. 1, and in **b**, the *black to white gray* scale represents the lowest value 0.1 to the highest value 0.9 of v

p ($p > p_c = 0.626$). To calculate the velocity, we selected two points along the propagating direction of waves. The time interval between u values of the two points reaching the maxima are recorded, and the velocity is the space between the two points divided by that time interval. The velocities in Fig. 6 are averages of 300 calculations. The dependence of the average velocity on p is shown in Fig. 6b. The velocity of the Ca^{2+} spiral wave increases with p, and the velocities are almost the same in the two types of media. To sum up, the discreteness and randomness do not prominently change the period and velocity of the Ca^{2+} spiral wave.

Many studies about Ca^{2+} waves pay attention to the discrete distribution of sites for Ca^{2+} release, where Ca^{2+} releasing sites are arranged on a regular grid (Falcke 2003; Shuai and Jung 2003). In RDM, not only are the active sites discretely distributed, but also the discrete sites are randomly arranged. Thus we must consider the question of whether the results we determined above are just a consequence of the discrete distribution of active sites or if the randomness also plays a significant role. To address this question, we compare the spiral waves in the systems where discrete active sites are regularly versus randomly arranged, i.e., RDM and RDcM. Here, p is fixed at 0.16, which is a physiologically reasonable value for *Xenopus* oocytes. First, the two systems are started from the initial condition as in Fig. 1. Obviously, the same results will be obtained for RDM. But in RDcM, for all $[IP_3]$, no similar spiral wave can be found as in the center row of Fig. 1, i.e., RDcM can not exhibit this mechanism of initiation of spiral wave without some unphysiological initial condition. We

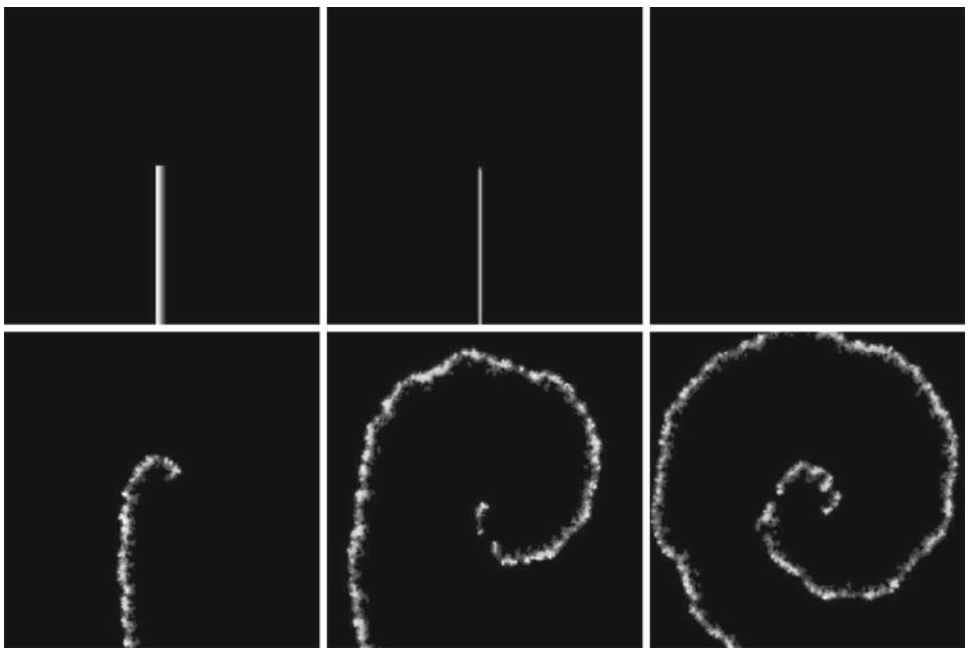

Fig. 4 Time sequence illustrating the process of spiral developing from initial condition for $p = 0.15$ and $[IP_3] = 0.4$ μM. *Top row* in HM, *bottom row* in RDM

Fig. 5 Time sequence illustrating the process of the spiral developing from an initial condition in the homogeneous medium for $p = 0.65$ and $[IP_3] = 0.4$ μM

conclude that the random distribution of the active sites is necessary for the spontaneous initiation of Ca^{2+} spiral waves, since the random distribution can improve the nonuniformity of the system, which has been proved to be an important factor for initiation of Ca^{2+} spiral waves.

Again, the two types of systems are started from locally perturbed rest states. The simulations show that Ca^{2+} spiral waves can be obtained in RDcM for 0.340 μM < $[IP_3]$ < 0.545 μM, and in RDM the region of $[IP_3]$ for spiral waves is slightly narrowed to 0.352 μM < $[IP_3]$ < 0.532 μM; clearly, this is not a significant difference. The velocity and

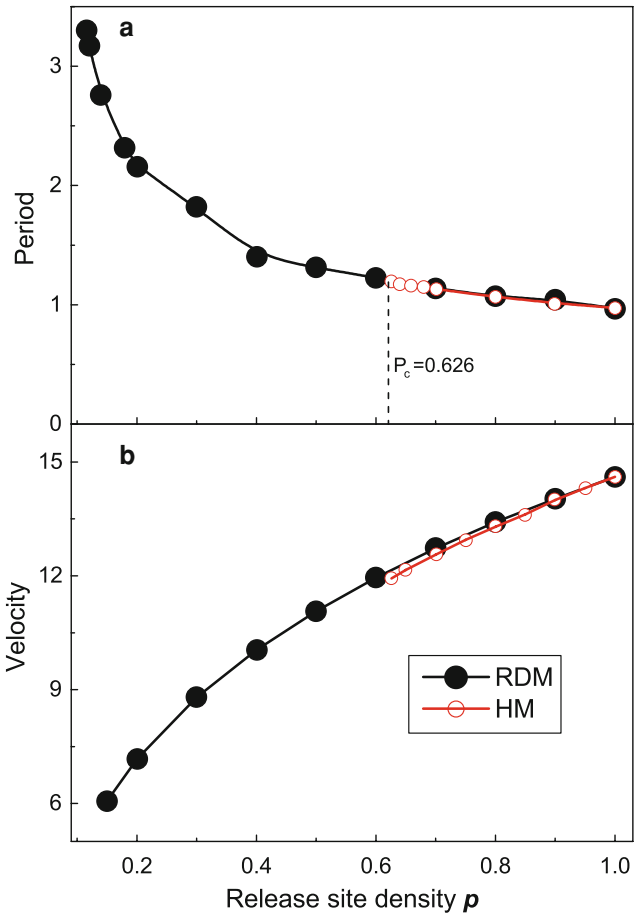

Fig. 6 Dependence of period (**a**) and velocity (**b**) of spiral waves on release site density p ($[IP_3] = 0.4$ μM)

period of spiral waves in the two types of media are compared in Fig. 7. It can be seen in Fig. 7a that the period decreases with $[IP_3]$ in both mediums, and this decrease is very similar to that shown in our previous work (Tang et al. 2008). In addition, the period does not vary significantly with the random distribution except for some fluctuation due to the randomness, and for enough large $[IP_3]$, the fluctuation disappears. In Fig. 7b, the velocity increases linearly with $[IP_3]$ in both media. It is interesting that, for low $[IP_3]$, the velocity of the spiral wave in RDM is less than that in RDcM. In contrast, for high $[IP_3]$, the RDM velocity is larger than the RDcM. Obviously, this is also a slight difference. The main difference between the two types of media is the fluctuation of distance between the active sites, i.e., in RDM, several active sites can cluster, and in some large areas, no active sites can be found. However, in RDcM, all active sites are isolated.

To explain Fig. 7b, three typical points are selected in RDM: P_{ua}, the center point of a large area with no active sites; P_{ca}, the center point of a large area totally occupied by active sites; and P_{ia}, the position of an isolated active site. The Ca^{2+} increase at the three points is compared in Fig. 8 for low (0.38 μM) and high (0.525 μM) $[IP_3]$. In Fig. 8, compared with P_{ia}, the refractory time of P_{ca} is reduced, which means an increase in the velocity of Ca^{2+} waves. In addition, this reduction in refractory time or increase in Ca^{2+} waves is more efficient for high $[IP_3]$ than lower $[IP_3]$. Otherwise, the refractory time of P_{ua} distinctly shows two phases of Ca^{2+} decay, which were also observed in *Xenopus* oocytes with high mitochondrial Ca^{2+} uptake (Falcke et al. 1999a). Compared with P_{ia}, this two-phase decay prolongs the refractory time of P_{ua}, correspondingly, the velocity of the Ca^{2+} wave is decreased. In contrast to P_{ca}, this decrease in velocity is more efficient for low $[IP_3]$ than higher $[IP_3]$. In Fig. 6b, for low $[IP_3]$, the decrease in velocity by P_{ua} in RDM is more efficient than the increase by P_{ca}, so the velocity of the Ca^{2+} wave is larger than that in RDcM, and vice versa.

Comparing RDcM and RDM shows that the random distribution of active sites is important for natural initiation (not initiation from unphysiological initial conditions) of spiral waves. But the randomness does not significantly

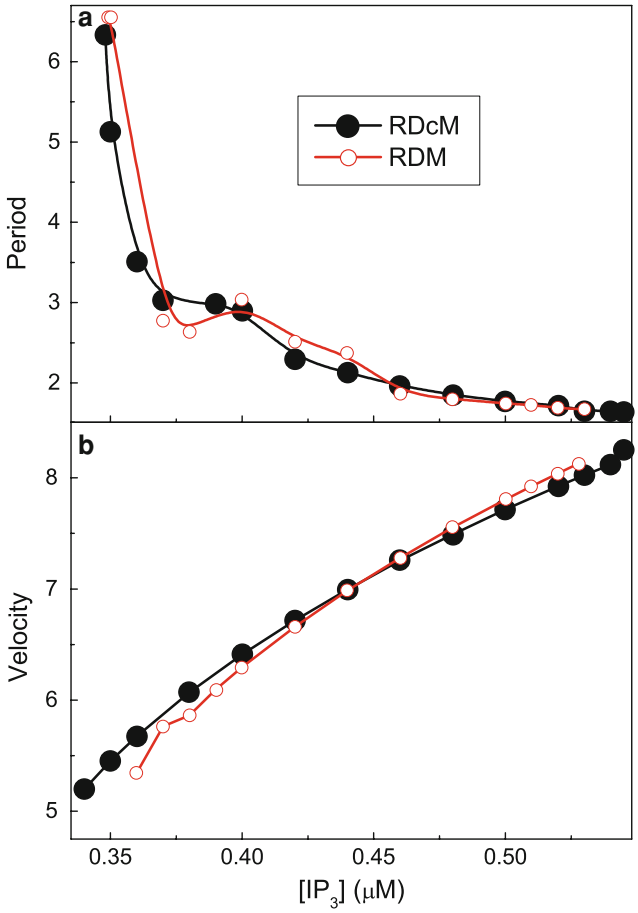

Fig. 7 Dependence of period (**a**) and velocity (**b**) of spiral waves on $[IP_3]$ ($p = 0.16$)

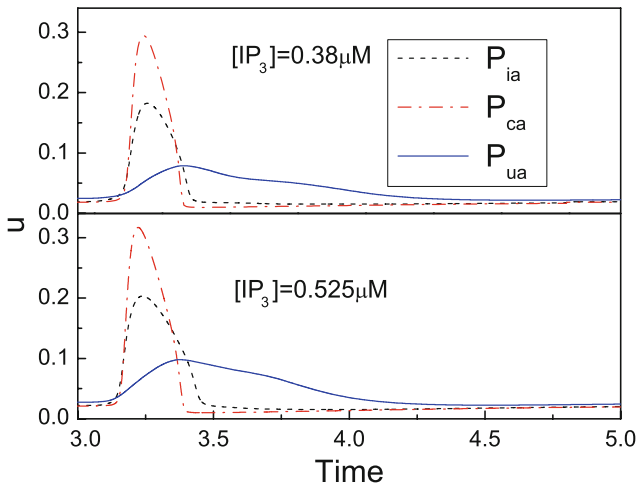

Fig. 8 Ca^{2+} increase at three typical points with high and low $[IP_3]$ ($p = 0.16$)

determine the characteristics, such as period and velocity, of the spiral waves, so when the initiation of spiral waves is not the issue of concern, the regular medium is an efficient model for Ca^{2+} waves.

Conclusions

In summary, we have compared the Ca^{2+} spiral waves in several types of media that differ mainly in the discrete and random distribution of ion channels in the ER. The results indicate that for lower $[IP_3]$, discrete and random distribution of ion channels exhibits a well-known mechanism for initiation of spiral waves. In HM, simulations show that the Ca^{2+} spiral wave can be obtained in the system only when the active site density $p > 0.626$, which is not a physiologically reasonable value. In contrast, the spiral wave can be obtained in the RDM at physiologically reasonable values of p. Furthermore, the comparison between RDcM and RDM shows that the random distribution of active sites is important for natural initiation of spiral waves. Period and velocity of Ca^{2+} spiral waves are not prominently changed by varying the type of medium.

The results are obtained based on a dimensionless Ca^{2+} model considering the exchange between the cytoplasm and the ER, which is also the main exchange in other Ca^{2+} models. This leads us to believe that similar results about the discrete and random distribution of ion channels can be found in other excitable Ca^{2+} models, such as the Tang–Othemer model (Tang et al. 1996).

Acknowledgments This work was supported by the National Natural Science Foundation of China under grant nos. 10875049 and 10747005, and the Key Project of Chinese Ministry of Education under no. 108096.

References

Bootman M, Niggli E, Berridge M, Lipp P (1997) Imaging the hierarchical Ca^{2+} signalling system in HeLa cells. J Physiol 499:307–314

Bugrim AE, Zhabotinsky AM, Epstein IR (1997) Calcium waves in a model with a random spatially discrete distribution of Ca^{2+} release sites. Biophys J 73:2897-2906. doi:10.1016/S0006-3495(97)78318-8

Cheng H, Lederer MR, Lederer WJ, Cannell MB (1996) Calcium sparks and $[Ca^{2+}]_i$ waves in cardiac myocytes. Am J Physiol (Cell Physiol) 270:C148–C159

De Young GW, Keizer J (1992) A single-pool inositol 1,4,5-trisphosphate-receptor-based model for agonist-stimulated oscillations in Ca^{2+} concentration. Proc Natl Acad Sci USA 89:9895–9899

Dupont G (1998) Theoretical insights into the mechanism of spiral Ca^{2+} wave initiation in Xenopus oocytes. Am J Physiol cell Physiol 275:C317–C322

Falcke M (2003) Deterministic and stochastic models of intracellular Ca^{2+} waves. New J phys 5:96.1–96.28

Falcke M (2004) Reading the patterns in living cells - the physics of ca^{2+} signaling. Adv in Phys 53:255–440 doi:10.1080/00018730410001703159

Falcke M, Hudson JL, Camacho P, Lechleiter JD (1999a) Impact of mitochondrial Ca^{2+}cycling on pattern formation and stability. Biophys J 77:37-44. doi:10.1016/S0006-3495(99)76870-0

Falcke M, Bär M, Lechleiter JD, Hudson JL (1999b) Spiral breakup and defect dynamics in a model for intracellular Ca^{2+} dynamics. Physica D 129:236-252. doi:10.1016/S0167-2789(98)00324-8

Falcke M, Li Y, Lechleiter JD, Camacho P (2003) Modeling the dependence of the period of intracellular Ca^{2+} waves on SERCA expression. Biophys J 85:1474-1481. doi:10.1016/S0006-3495(03)74580-9

Foskett JK, White C, Cheung K, Mak DD (2007) Inositol Trisphosphate Receptor Ca^{2+} Release Channels. Physiol Rev 87:593-658. doi:10.1152/physrev.00035.2006

Harris-White ME, Zanotti SA, Frautschy SA, Charles AC (1998) Spiral Intercellular Calcium Waves in Hippocampal Slice Cultures. J Neurophysiol 79:1045–1052

Lechleiter JD, Girard S, Peralta E, Clapham D (1991a) Spiral calcium wave propagation and annihilation in Xenopus laevis oocytes. Science 252:123-126. doi:10.1126/science.2011747

Lechleiter JD, Girard S, Clapham D, Peralta E (1991b) Subcellular patterns of calcium release determined by G protein-specific residues of muscarinic receptors. Nature 350:505-508. doi:10.1038/350505a0

Li YX, Rinzel J (1994) Equations for $InsP_3$ Receptor-mediated $[Ca^2]_i$ Oscillations Derived from a Detailed Kinetic Model: A Hodgkin-Huxley like formalism. J Theor Biol 166:461-473. doi:0022-5193/94/040461+13

Lipp P, Niggli E (1993) Microscopic spiral waves reveal positive feedback in subcellular calcium signaling. Biophys J 65:2272-2276. doi:10.1016/S0006-3495(93)81316-X

Parker I, Yao Y (1991) Regenerative Release of Calcium from Functionally Discrete Subcellular Stores by Inositol Trisphosphate. Proc R Soc Lond B 246: 269–274

Parker I, Yao Y (1996) Ca^{2+} transients associated with openings of inositol trisphosphate-gated channels in Xenopus oocytes. J Physiol 491: 663–668

Ridgway EB, Gilkey JC, Jaffe LF (1977) Free calcium increases explosively in activating medaka eggs. Adv in Phys 74:623-627

Robb-Gaspers LD, Thomas AP (1995) Coordination of Ca^{2+} signaling by intercellular propagation of Ca^{2+} waves in the intact liver. J Biol Chem 270:8102–8107

Sanderson MJ, Charles AC, Boitano S, Dirksen ER (1994) Mechanisms and function of intercellular calcium signaling. Mol Cell Endocrinol 98:173–187

Shuai JW, Jung P (2003) Sub-threshold Ca^{2+} waves. New J Phys 5:132.1–132.20

Tang Y, Stephenson JL, Othmer HG (1996) Simplification and analysis of models of calcium dynamics based on IP_3-sensitive calcium channel kinetics. Biophys J 70:246-263. doi:10.1016/S0006-3495(96)79567-X

Tang J, Jia Y, Ma J, Yi M (2008) Numerical study of IP_3-dependent Ca^{2+} spiral waves in Xenopus oocytes. Europhys Lett 83:68001. doi:10.1209/0295-5075/83/68001

Thomas AP, Robb-Gaspers LD, Rooney TA, Hajnoczky G, Renard-Rooney DC, Lin C (1995) Spatial organization of oscillating calcium signals in liver. Biochem Soc Trans 23: 642–648

Yao Y, Choi J, Parker I (1995) Quantal puffs of intracellular Ca^{2+} evoked by inositol trisphosphate in Xenopus oocytes. J Physiol 482:533–553

Yagodin S, Holtzclaw LA, Sheppard CA, Russell JT (1994) Nonlinear propagation of agonist-induced cytoplasmic calcium waves in single astrocytes. J Neurobiol 25:265-280. doi:10.1002/neu.480250307

Yagodin S, Holtzclaw LA, Russell JT (1995) Subcellular calcium oscillators and calcium influx support agonist-induced calcium waves in cultured astrocytes. Mol Cell Biochem 149/150: 137-144. doi:10.1007/BF01076572